Analyst

Cite this: *Analyst*, 2012, **137**, 1259

www.rsc.org/analyst

PAPER

Streptococcus suis II immunoassay based on thorny gold nanoparticles and surface enhanced Raman scattering†

Kun Chen, Heyou Han* and Zhihui Luo

Received 22nd October 2011, Accepted 27th December 2011
DOI: 10.1039/c2an15997j

An immunoassay based on surface enhanced Raman scattering (SERS) spectroscopy was developed to detect muramidase released protein (MRP) antibody against *Streptococcus suis* II (SS2) utilizing thorny gold nanoparticles (tAuNPs) as SERS substrates. Initially, tAuNPs with multi-branches were prepared by the seed-mediated growth method in the absence of templates and surfactants, facilitating *p*-mercaptobenzoic acid (*p*MBA) conjugation covalently onto the tAuNPs through S–Au bonds. The obtained immuno-SERS tag affording strong Raman signals made it possible to establish an application of indirect detection of the MRP antibody against SS2 with a sandwich assay at a highly sensitive level. The Raman intensity at 1588 cm^{-1} was proportional to the logarithm of the concentration of MRP antibody in the range of 10 pg mL^{-1} to 0.1 μg mL^{-1}. The detection sensitivity was significantly improved to 0.1 pg mL^{-1} by using the immuno-SERS tags. Furthermore, the proposed SERS approach was applied to detect MRP antibody in pig serum samples, and the results agreed well with those of ELISA, indicating great potential for clinical application in diagnostic immunoassays.

Introduction

Streptococcus suis (*S. suis*), a gram-positive, facultative anaerobic coccus, has been implicated as the cause of a wide range of clinical diseases. In nearly all countries with a large-scale pig industry, *S. suis* causes a rapidly progressive, even fatal sepsis in infant pigs, associated with meningitis, polyarthritis, and occasionally, pneumonia.[1] It is also a zoonotic disease, capable of transmission to humans from pigs[2] upon occupational exposure. Human infections can be severe, with meningitis, endocarditis, septicaemia, pneumonia, and deafness as possible outcomes of infection.[3–6] One of the most common infections is from *S. suis* type 2 (SS2), which has received much attention since an outbreak in Sichuan, China.[4,7] The serotype of SS2 is the most frequently associated with disease, hence many studies have concentrated on its detection as well as that of its virulence factors.[8] Muramidase released protein (MRP) is one of two main virulence factors separated from SS2. The strains of SS2 which produce MRP are frequently isolated from organs of diseased pigs,[9] so virulence factor MRP is used often as a specific clinical sign of pig diseases.

Serological evidence of SS2 exposure, including enzyme linked immunosorbent assay (ELISA), are usually collected for SS2 detection and diagnosis. When distinguishing between different SS serotypes or different strains of the same serotype by biological assay methods, their biochemical reactions are quite different, so artificial negative is constant. Generally, they are used as a supplementary identification. Molecular diagnoses can improve the efficiency and accuracy of the identification results,[9,10] and therefore they are suitable for epidemiological investigations, providing effective detection methods for confining the spread of SS disease.[11] These analytical methods play a certain role in SS disease detection and diagnosis; however, they are susceptible to interference, time-consuming, cumbersome in operation and prone to false-positive reactions. In order to improve the diagnostic procedures for SS2, new techniques should be explored to establish accurate and rapid detection methods for monitoring and controlling the disease, and especially for the exploration of pathogenic disease mechanisms.

In contrast to normal analytical methods, Raman scattering can provide qualitative and quantitative information through the narrow and distinguishable molecular vibrational bands for real-time *in situ* monitoring detection and imaging.[12–15] Surface-enhanced Raman scattering (SERS) has pushed this technology forward to micro or trace analysis and the assay of biological molecules.[16,17] The enhancement factor on nanoscale roughed metal surfaces reaches as much as 10^{14}–10^{15}, which allows the technique to be sensitive enough to detect single molecules.[18–20] Most notably, aqueous samples under physiological conditions can be analyzed based on SERS, with little interference from water. In addition, SERS analysis is rarely hindered by oxygen, humidity and other interferences, and is suggested to be a favorable method for sensitive biological identification and determination. A series of sensitive and selective detection

College of Science, State Key Laboratory of Agricultural Microbiology, Huazhong Agricultural University, Wuhan, 430070, China. E-mail: hyhan@mail.hzau.edu.cn; Fax: +86 027 87288246; Tel: +86 027 87288246
† Electronic supplementary information (ESI) available. See DOI: 10.1039/c2an15997j

methods based on SERS have been developed for biological assays.[21–23] Among them, gold nanoparticles (AuNPs) have become one of the most favored SERS substrates because of their superior properties, such as facile synthesis, tunable particle size, extensive stability, and biocompatibility. AuNPs as adaptable and versatile carriers for the immobilization of antibodies or antigens were initially utilized by Porter and co-workers in immunoassay readout.[24] Since then, numerous new immune protocols have emerged based on SERS, employing diverse forms of gold nanostructures, particles and films, or bimetal nanoassemblies.[25–27]

In this study, we describe a nanoparticle-based sandwich-type immunoassay for MRP antibody detection utilizing thorny gold nanoparticles (tAuNPs) fabricated with the rabbit anti-pig IgG as immuno-SERS tags, as shown in Scheme 1. The tAuNPs used as SERS substrates were synthesized by a seed-mediated growth method in the absence of templates and surfactants. Hence, the tAuNPs have prominent advantages over conventional SERS substrates: facile synthesis, convenient modification, good biocompatibility and equal SERS effect. The immuno-SERS tags were assembled by linking the tAuNPs and a secondary antibody together with *p*-mercaptobenzoic acid (pMBA), and successfully applied to the specific detection of the MRP antibody in pig serum samples.

Experimental

Chemicals and materials

1-Ethyl-3-[3-(dimethylamino)propyl]carbodiimide (EDC) and *p*-mercaptobenzoic Acid (*p*MBA) were obtained from Tokyo Chemical Industry Co., Ltd. Rabbit anti-pig IgG and rabbit anti-mouse IgG were purchased from Shanghai Bio Life Science & Technology Co., Ltd. Pig serum samples, MRP, Porcine Circovirus type 2 (PCV2), Porcine Reproductive and Respiratory Syndrome virus (PRRSV), ApxIV of *Actinobacillus pleuropneumoniae* and their corresponding monoclonal antibodies were kindly provided by State Key Laboratory of Agricultural Microbiology (Wuhan, China). All other reagents were from Sinopharm Chemical Reagent Co. Ltd and were used as received without further purification. Ultrapure deionized water was used throughout the experiments.

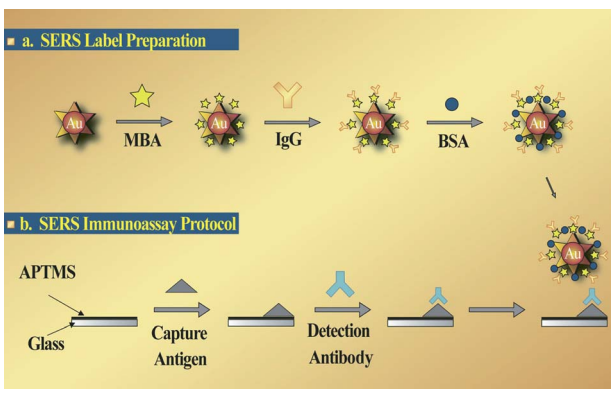

Scheme 1 Scheme of SERS immunoassay by immunogold nanotags. (a) *p*MBA links rabbit anti-pig IgG and tAuNPs together, and BSA is co-immobilized on *p*MBA-tAuNPs to block the residual part of the immunocomplex surface. (b) Sandwich immunoassay process based on SERS labeled immunogold nanotags for MRP antibody.

Instrumentation

The SERS spectra were obtained using an inVia Raman spectrograph (Renishaw, UK) equipped with a co-focusing microscope (Leica, Germany). A He–Ne laser (633 nm) was used as the excitation source with a laser power of approximately 1.7 mW on the sample. The band of a silicon wafer at 520 cm^{-1} was used to calibrate the Raman spectrograph. The SERS spectra were obtained with an exposure time of 10 s and one time accumulation. The UV-vis absorption spectra were acquired using a Thermo Nicolet 300 UV-vis spectrometer (Thermo Nicolet, USA). Transmission electron microscopy (TEM) images were obtained using a Tecnai G20 microscope (FEI, Czech Republic).

Preparation of thorny gold nanoparticles

Gold seeds with average diameters of 24 nm were synthesized through the citrate-mediated reduction of $HAuCl_4$. Briefly, 100 mL of 0.3 mM $HAuCl_4$ solution was refluxed under stirring. 5 mL of 38.8 mM sodium citrate was rapidly added to the boiling solution. After the color changed to red, the solution was heating for another 30 min and was allowed to cool to room temperature. The gold seeds were filtered, and the resulting nanoparticles were characterized by transmission electron microscopy (TEM) and UV-vis absorption spectroscopy.

The tAuNPs were prepared by a seed-mediated growth process using AuNPs of a small size as growth seeds.[28] An aqueous solution of $HAuCl_4$ (0.25 mM, 50 mL) was vigorously stirred, and NH_2OH solution (40 mM, 1 mL), $AgNO_3$ solution (1.0 mM, 0.1 mL) and gold seeds (0.1 mL) were added sequentially, resulting in a change in the solution color from pale yellow to blue, and brownish blue afterwards. The final color change indicated that the tAuNPs were generated.

Preparation of *p*MBA labeled immunogold nanocomplexes

Under vigorous stirring, 10 μL *p*MBA was added into 1 mL suspension of tAuNPs to a final concentration of 0.05 μM. After 30 min at room temperature, the *p*MBA-tAuNPs were purified and washed by centrifugation at 6000 rpm for 15 min to remove free *p*MBA, and re-suspended in 1 mL PBS (0.01 M, pH 7.0) solution. Typically, the *p*MBA-tAuNPs were firstly immersed into 1% (w/w) EDC in anhydrous acetonitrile for 5 h to activate the free carboxyl groups of *p*MBA by forming an O-acylurea intermediate with EDC. 50 μL rabbit anti-pig IgG solution (100 μg mL^{-1} in 0.01 M PBS) was slowly added to the suspension of *p*MBA-tAuNPs, and incubated at 37 °C for 1 h.[29,30] The excess IgG was removed by centrifugation at 6000 rpm for 15 min. After washing, 1 mL BSA (1% in PBS) was added into the solution to block the residual vacant portion of the *p*MBA-tAuNPs surface. The IgG-*p*MBA-tAuNPs were then separated from the mixture, thoroughly washed by centrifugation, and resuspended in 1 mL PBS (0.01 M, pH 7.0) solution. The immuno-SERS tags obtained were stored below 4 °C prior to use.

SERS immunoassay protocol

The SERS immunoassay was performed on glass slides. These specially cleaned glass slides were placed in a dilute solution of 3-aminopropyltrimethoxysilane (APTMS) (4 g APTMS in 36 g CH_3OH) for 12 h and rinsed with abundant amounts of CH_3OH and H_2O in turn.[31] The SERS-based immunoassay was carried out *via* a sandwich immunosorbent assay process. 50 μL MRP was immobilized onto the glass slide and formed a monolayer specific for the MRP antibody. After removing the solution, the MRP-immobilized substrate was washed with PBS and blocked with BSA. MRP antibody solutions with concentrations ranging from 1 μg mL^{-1} to 0.1 pg mL^{-1} were prepared by serial dilution with PBS buffer, piped onto the immunoassay substrate, and incubated at 37 °C for 2 h. After rinsing with PBT (0.01 M PBS and 0.05% Tween-20) to remove physically non-absorbed MRP antibody, the substrate was incubated with 50 μL IgG-*p*MBA-tAuNPs suspension for 2 h at 37 °C. All samples were then carefully rinsed with PBT and stored at 4 °C prior to SERS measurements.

ELISA protocol

MRP (100 μL, 2.5 μg mL^{-1} in PBS) was added into each microwell of a 96-well microtiter plate and maintained overnight at 4 °C. After washing with PBT, 100 μL serial dilutions of pig serum were introduced into the wells coated with MRP at 37 °C for 1.5 h and washed with PBT, followed by addition of 100 μL per well of IgG-horseradish peroxidase (IgG-HRP) solution to perform the sandwich-type immunoreactions. After incubation for 30 min with gentle shaking at 37 °C, the plates were washed and underwent another incubation for 30 min at room temperature. The color development was stopped with 1 M HCl (50 μL per well), and the absorbance was obtained at 450 nm using a Thermo Scientific Multiskan Spectrum. The results were compared with those measured by SERS.

Results and discussion

Characterization of SERS tags

The two-step assembly process of the MBA-labeled tAuNPs was monitored by UV-vis absorption spectroscopy (Fig. 1), and the morphology of the tAuNPs was verified by TEM (Fig. 2). The

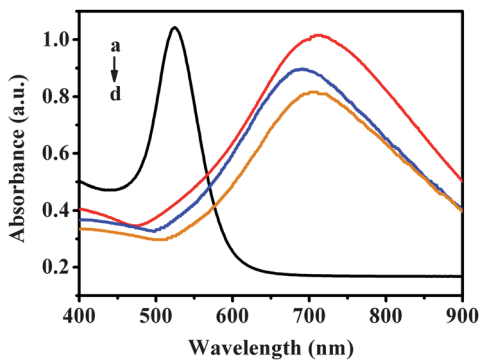

Fig. 1 UV-vis absorption spectra of Au seeds (a), tAuNPs (b), *p*MBA-tAuNPs (c) and IgG-*p*MBA-tAuNPs (d).

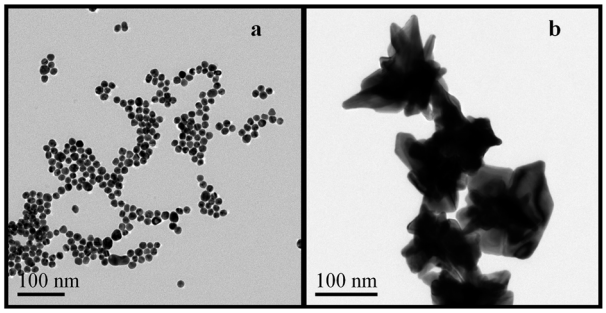

Fig. 2 TEM images of Au seeds (a) and pMBA-tAuNPs (b).

UV-vis spectrum of the gold seeds showed a peak arising at 522 nm, which was consistent with the surface plasmon band of AuNPs with a diameter around 24 nm (Fig. 1, a). After non-template seed-mediated growth, the surface plasmon band of the obtained tAuNPs broadened and shifted from 522 nm to 708 nm (Fig. 1, line b), indicating the central parts of the nanostructures expanded and the nanothorns on one gold nanoparticle elongated (Fig. 2).[32,33]

The thorny gold nanoparticles were synthesized at room temperature, by sequentially adding $AgNO_3$, reductant and gold seeds to the reaction system. Without any surfactant, and with no need to precisely control the reaction conditions, the synthesis of thorny gold nanoparticles was easily carried out, indicating this is one of their advantages. Because we did not use any surfactant, such as CTAB or PVP, which are the most commonly employed reagents in nonspherical nanoparticle synthesis, the thorny gold nanoparticles were modified directly without the need for further washing steps for template removal.

When the *p*MBA solution was mixed with the tAuNPs solution, *p*MBA attached to the surface of tAuNPs by strong thiol–Au bonding. After tAuNPs were coated with *p*MBA, the surface of gold nanoparticles was not as rough. This could be attributed to the washing steps, when the long thorns were gradually lost. Most long thorns were mechanically stripped from the main body during several rounds of centrifugation, leading to the obtained *p*MBA-tAuNPs having greater symmetry than before. Consequently, after the modification of tAuNPs with *p*MBA, the plasmon resonance peak of *p*MBA-tAuNPs showed a blue shift from 708 nm to 689 nm (Fig. 1, line c). Nevertheless, when IgG was added to the MBA-tAuNPs solution, the plasmon resonance peak of immuno-SERS tags shifted to 702 nm, as the IgG was immobilized with a more or less uniform thickness over the entire surface of the particle (Fig. 1, line d). The gradual decrease of absorbance was attributed to the loss *via* centrifugation after each washing step.

SERS performance of SERS tags and immuno-SERS tags

The SERS behavior of the immuno-complex was then tested (Fig. 3). It is known that optical hot spots are frequently formed at the junctions or gaps between nanostructures.[34–36] Similarly, increased fields are also found on the surface of anisotropic AuNPs with sharp features,[37] such as gold nanostars and tAuNPs. The plasmons of a gold nanoparticle with tips result from hybridization of plasmons of the core and tips of the nanoparticle. The cross section for excitation of the bonding

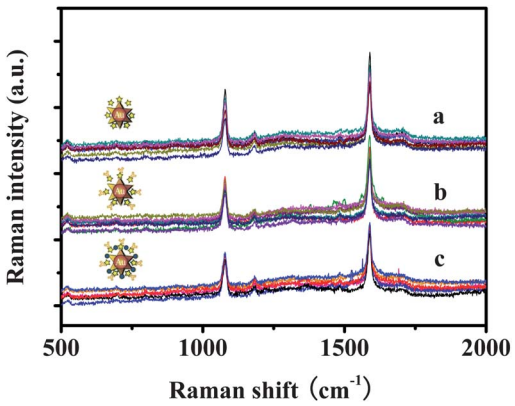

Fig. 3 Typical SERS spectra ($n = 7$) of *p*MBA-tAuNPs (a), IgG-*p*MBA-tAuNPs (b) and BSA blocked IgG-*p*MBA-tAuNPs (c).

plasmons is dramatically increased by the mixing in the core plasmon mode, resulting in very large local electric field enhancements. Therefore, anisotropic AuNPs are superior in producing more strongly enhanced Raman modes than spherical AuNPs or gold nanorods, which make them promising additions to the family of SERS substrates.[38] In addition, the surface area of the tAuNP is larger than that of a symmetric nanosphere of the same size, and as a result of that more *p*MBA can be fixed to each tAuNP for providing distinguishable SERS signals at ultralow concentrations. Here, *p*MBA was used not only as a sign reporter of SERS because it was capable of forming a well-defined monolayer on the gold surface with a characteristic molecular footprint, but also as a linker for fixing the secondary antibody (rabbit anti-pig IgG) onto tAuNPs. Two sharp SERS peaks were obtained from all *p*MBA-labeled nanocomplexes, and the peaks at 1588 cm^{-1} could be assigned to symmetric C–C stretching vibrations (Fig. 3, a). After immobilization of IgG and BSA, similar SERS patterns were observed reproducibly (Fig. 3, b and c). Some tiny peak shifts showed that *p*MBA bound to IgG was relative to those from *p*MBA bound to tAuNPs. These changes might be attributed to the bond formation between *p*MBA and IgG on the diverse tAuNP surface.

Immune analyses of MRP antibody

In an indirect sandwich immunoassay, the detection sensitivity is mainly dominated by the performance of the capture antigen and secondary antibody, and the detection signal critically depends on the number of secondary antibody-conjugated SERS tags. To achieve an ultrahigh sensitivity, we improved the SERS assay by optimizing the concentration of capture antigen and ratio of rabbit anti-pig IgG relative to *p*MBA-tAuNPs (Fig. S1 and S2, ESI†). According to the obtained data, a capture antigen concentration of 2.5 μg mL^{-1} and IgG volume of 50 μL were used in the following experiments.

Representative SERS spectra collected for MRP antibody showed the dependence of SERS intensity on antibody concentration (Fig. 4A). The peak intensity at 1588 cm^{-1} was proportional to the number of immuno-SERS tags, and we used the characteristic Raman band at 1588 cm^{-1} to estimate the concentrations of antibody (Fig. 4B). A sigmoidal line was generated by a curve fit using the Hill equation [eqn (1)], where θ refers to the fraction of ligand binding sites filled, $[L]$ is the ligand concentration, K_A is the ligand concentration producing half occupation, and n is the Hill coefficient.

$$\theta = \frac{[L]^n}{(K_A)^n + [L]^n} \quad (1)$$

The Raman intensity increased exponentially with the amount of detected antibody. The middle part of the corresponding calibration curve showed a linear relationship between the Raman intensity and the logarithmic value of antibody concentration ranging from 0.1 μg mL^{-1} to 10 pg mL^{-1} (Fig. 4B). BSA of 1 μg mL^{-1} was used as a negative control to obtain a blank spectrum and examine the nonspecific adsorption by replacing the target protein. A small minority of control spectra showed weak peaks at the same position as *p*MBA, indicating some nonspecific binding in the immunoassay. The average SERS intensity obtained from 0.1 pg mL^{-1} MRP antibody was three times greater than the control (Fig. 5). In fact, the absorption behavior indicated monolayer absorption during each step of the immunoassay. Also, the distribution of the antibody was symmetric at a concentration of 0.1 pg mL^{-1} in a 20 × 20 μm^2 area where SERS spectra was collected randomly at seven different spots. As a result, the confidence limit of detection was set at a creditable level of 0.1 pg mL^{-1}.

Immunoassay of MRP antibody in pig serum

To demonstrate the feasibility of the proposed method, we examined a number of diluted serum samples from SS2 positive pigs, as well as control samples (from pigs that did not contract SS2 infection). Fig. 4C outlines the SERS immunoassay for the detection of MRP in clinical diagnosis of SS2. The direct SERS spectra of MRP antibody adsorbed on the tAuNPs (Fig. 4C, a) showed that, although the concentration of MRP antibody was as high as 1 μg mL^{-1}, the signal was weak and prone to environmental perturbation. There were obvious differences between direct SERS spectra of positive and negative serum samples (Fig. 4C, b and c). The serum from a healthy pig seemed cleaner than the serum from an infected pig. The differences indicated the sample individual suffered some disease related to blood abnormality. With the SERS immune label, the SERS intensity of the Raman reporter was notably larger than that of MRP or positive serum, even the tested serum 1000-fold diluted (Fig. 4C, d). The result demonstrates that, based on immune recognition, the SERS-based method using tAuNPs provides practical evidence for diagnosis of SS2 disease and selective and sensitive measurement of antibodies to MRP of SS2 in pig serum.

The specificity of the SERS immunoassay was studied by analysing three other pathogenic microorganisms associated with pigs. Fig. 6 shows the mean responses of the SERS-based assay to 100-fold diluted serum corresponding to MRP, PCV2, PRRSV and ApxIV. As expected, the MRP serum yielded the most intense signals, while the others only exhibited weak signals, similar to those of their negative controls. The apparent SERS intensity differences between positive and negative for SS2 *versus* other pathogenic microorganisms (Fig. 6) clearly suggested that the SERS immunoassay was able to recognise pig serums infected by SS2. To further demonstrate the specificity of the proposed approach for MRP antibody analysis, rabbit

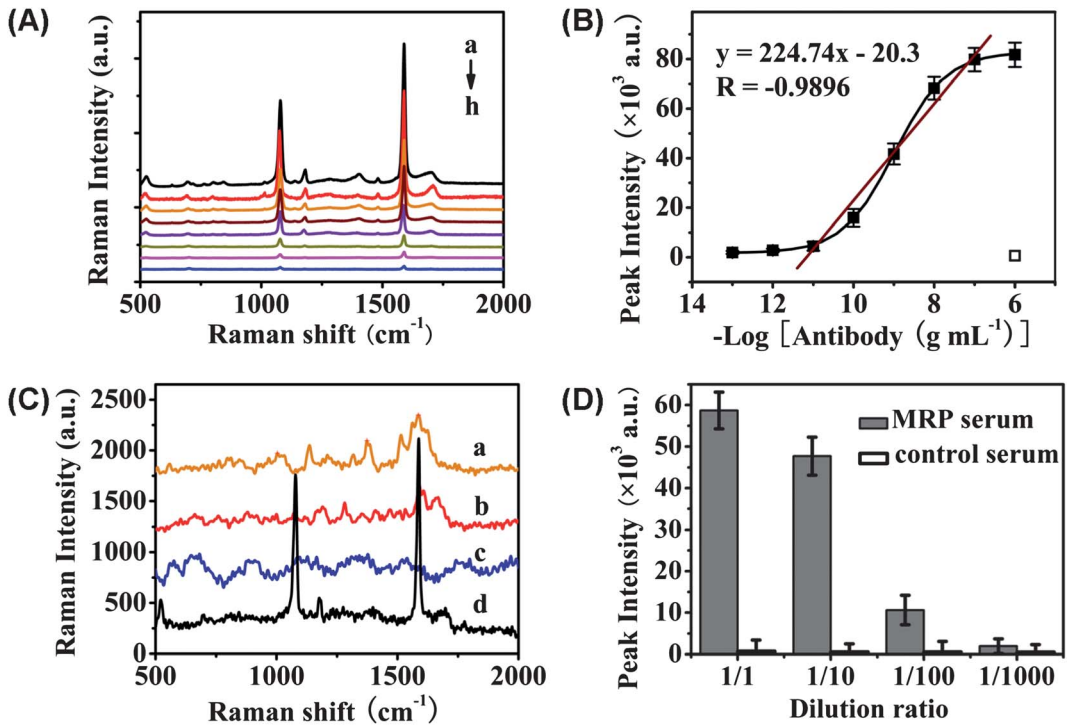

Fig. 4 SERS-based immunoassay for MRP antibody. (A) SERS immunoassay for MRP detection at different concentrations from 1 μg mL^{-1} to 0.1 pg mL^{-1} (a–g); (B) Corresponding dose–response curves for SERS-based (solid squares) detection of MRP. Each point depicted the average measurements of seven. BSA (1 μg mL^{-1}) was used as a negative control (open square); (C) SERS immunoassay for the detection of MRP antibody in pig serum samples: SERS spectrum of MRP antibody (1 μg mL^{-1}) (a), negative serum (b), positive serum (c), and positive serum (1000 times diluted) using *p*MBA-labeled immunogold nanocomplexes (d); (D) Histogram of mean intensity ($N = 7$) at different serum dilution ratios in the SERS assays. Error bars were calculated based on the standard deviation of seven measurements.

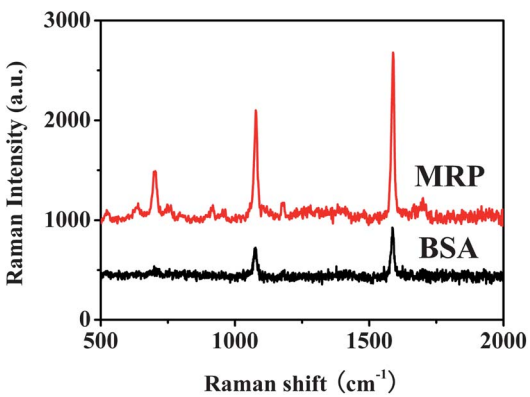

Fig. 5 Responses of the SERS-based immunoassay to 1 μg mL^{-1} BSA (black line) and 0.1 pg mL^{-1} MRP antibody (red line).

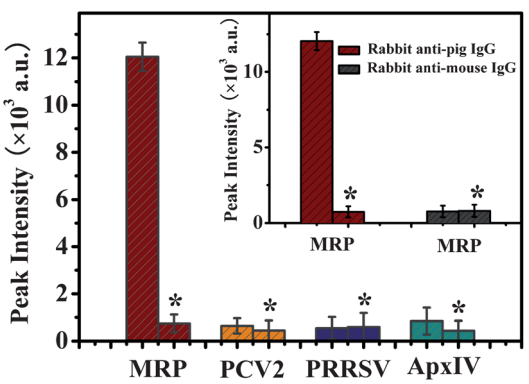

Fig. 6 Histogram of mean intensity ($N = 7$) in the SERS immunoassay for MRP (red), PCV2 (yellow), PRRSV (blue) and ApxIV (green). *: the negative controls for each positive serum sample. Inset: comparison of SERS tags coated with rabbit anti-pig IgG (red) and rabbit anti-mouse IgG (black) in the SERS immunoassay for MRP. All the serum samples were 100-fold diluted.

anti-mouse IgG was used to coat *p*MBA-tAuNPs, substituting for rabbit anti-pig IgG to assemble the SERS tags. The results indicate that the nonspecific interaction of rabbit anti-pig IgG with the MRP antibody was also negligible (Fig. 6, inset).

To estimate the diagnostic performance of the proposed method, 36 clinical serum samples collected from infected pigs were analyzed by both the SERS immune method and ELISA without any reference test to classify pigs as truly infected or non-infected. The results were shown in Table 1. Compared with ELISA, the proposed method has a higher sensitivity and specificity for the detection of MRP antibody of SS2: high efficiency (91.6%), high sensitivity (94.4%), high specificity (88.9%), moderate false-positive rate (11.1%) and low false-negative rate (5.5%). The high percentage of agreement (91.6%) between the SERS assay and ELISA demonstrates that the present method provides significant advantages in practical or clinical application.

Table 1 Comparative data of the SERS assay and indirect ELISA of 36 pig serum samples

		Indirect ELISA			Performance				
		Positive	Negative	Total	Efficiency[a]	Sensitivity[b]	Specificity[c]	False-positive rate[d]	False-negative rate[e]
SERS Assay	Positive	17	2	19	91.6%	94.4%	88.9%	11.1%	5.5%
	Negative	1	16	17					
	Total	18	18	36					

[a] Efficiency = (True-positive + True-negative) × 100%/Total. [b] Sensitivity = True-positive × 100%/(True-positive + False-negative). [c] Specificity = True-negative × 100%/(True-negative + False-positive). [d] False-positive = False-positive × 100%/(True-positive + False-negative). [e] False-negative = False-negative × 100%/(True-positive + False-negative).

Conclusions

In summary, we reported a sensitive and selective SERS immunoassay to detect and quantify MRP antibody against epidemic disease SS2. The SERS assay exhibited a good linear relationship between the logarithm of target concentration and the SERS signal of *p*MBA at 1588 cm^{-1} over a concentration range of four orders of magnitude (10 pg mL^{-1} to 0.1 μg mL^{-1}). By using the versatile tAuNPs, the SERS immunoassay showed high sensitivity and specificity towards the MRP antibody with a detection limit of 0.1 pg mL^{-1}. Serum sample detection demonstrated a high agreement rate with the traditional method. The proposed method will promote research on detection of SS2 and will take an ulterior step to prevent or control the spread of *Streptococcus suis* II disease. Furthermore, the SERS-based analytical method could be extended to other zoonotic diseases by changing the labeling strategy, and multiple detection is available for borne disease analysis and screening.

Acknowledgements

The authors gratefully acknowledge the support for this research by the National Natural Science Foundation of China (20975042, 21175051), the Fundamental Research Funds for the Central Universities of China (2010PY009, 2011PY139), the Natural Science Foundation of Hubei Province Innovation Team (2011CDA115) and Genetically Modified Major Projects (2009ZX08012-015B).

References

1 S. Sriskandan and J. D. Slater, *PLoS Med.*, 2006, **3**, 595–597.
2 Y. Huang, L. Teng, S. Ho and P. Hsueh, *J. Microbiol. Immunol. Infect.*, 2005, **38**, 306–313.
3 Z. R. Lun, Q. P. Wang, X. G. Chen, A. X. Li and X. Q. Zhu, *Lancet Infect. Dis.*, 2007, **7**, 201–209.
4 D. Normile, *Science*, 2005, **309**, 1308–1309.
5 H. F. Wertheim, H. D. Nghia, W. Taylor and C. Schultsz, *Clin. Infect. Dis.*, 2009, **48**, 617–625.
6 M. Segura, *J. Infect. Dis.*, 2009, **199**, 4–6.
7 C. Ye, X. Zhu, H. Jing, H. Du, M. Segura, H. Zheng, B. Kan, L. Wang, X. Bai, Y. Zhou, Z. Cui, S. Zhang, D. Jin, N. Sun, X. Luo, J. Zhang, Z. Gong, X. Wang, L. Wang, H. Sun, Z. Li, Q. Sun, H. Liu, B. Dong, C. Ke, H. Yuan, H. Wang, K. Tian, Y. Wang, M. Gottschalk and J. Xu, *Emerging Infect. Dis.*, 2006, **12**, 1203–1208.
8 M. Gottschalk and M. Segura, *Vet. Microbiol.*, 2000, **76**, 259–272.
9 H. E. Smith, U. Vecht, H. J. Wisselink, N. Stockhofe-Zurwieden, Y. Biermann and M. A. Smits, *Infect. Immun.*, 1996, **64**, 4409–4412.
10 H. J. Wisselink, J. J. Joosten and H. E. Smith, *J. Clin. Microbiol.*, 2002, **40**, 2922–2929.
11 C. Marois, S. Bougeard, M. Gottschalk and M. Kobisch, *J. Clin. Microbiol.*, 2004, **42**, 3169–3175.
12 A. Das, S. Pisana, B. Chakraborty, S. Piscanec, S. K. Saha, U. V. Waghmare, K. S. Novoselov, H. R. Krishnamurthy, A. K. Geim, A. C. Ferrari and A. K. Sood, *Nat. Nanotechnol.*, 2008, **3**, 210–215.
13 Z. Ioffe, T. Shamai, A. Ophir, G. Noy, I. Yutsis, K. Kfir, O. Cheshnovsky and Y. Selzer, *Nat. Nanotechnol.*, 2008, **3**, 727–732.
14 T. M. Barnard and N. E. Leadbeate, *Chem. Commun.*, 2006, 3615–3616.
15 B. G. Saar, C. W. Freudiger, J. Reichman, C. M. Stanley, G. R. Holtom and X. S. Xie, *Science*, 2010, **330**, 1368–1370.
16 J. T. Golab, J. R. Sprague, K. T. Carron, G. C. Schatz and R. P. Van Duyne, *J. Chem. Phys.*, 1988, **88**, 7942–7951.
17 M. G. Albrecht and J. A. Creighton, *J. Am. Chem. Soc.*, 1977, **99**, 5215–5217.
18 S. Nie and S. R. Emory, *Science*, 1997, **275**, 1102–1106.
19 K. Kneipp, Y. Wang, H. Kneipp, L. T. Perelman, I. Itzkan, R. R. Dasari and M. S. Feld, *Phys. Rev. Lett.*, 1997, **78**, 1667–1670.
20 X. M. Qian and S. M. Nie, *Chem. Soc. Rev.*, 2008, **37**, 912–920.
21 I. A. Larmour and D. Graham, *Analyst*, 2011, **136**, 3831–3853.
22 M. D. Porter, R. J. Lipert, L. M. Siperko, G. Wang and R. Narayanana, *Chem. Soc. Rev.*, 2008, **37**, 1001–1011.
23 R. A. Alvarez-Puebla and L. M. Liz-Marzán, *Small*, 2010, **6**, 604–610.
24 J. Ni, R. J. Lipert, G. B. Dawson and M. D. Porter, *Anal. Chem.*, 1999, **71**, 4903–4908.
25 S. M. Asiala and Z. D. Schultz, *Analyst*, 2011, **136**, 4472–4479.
26 T. Kang, S. M. Yoo, I. Yoon, S. Y. Lee and B. Kim, *Nano Lett.*, 2010, **10**, 1189–1193.
27 X. Liu, M. Knauer, N. P. Ivleva, R. Niessner and C. Haisch, *Anal. Chem.*, 2010, **82**, 441–446.
28 H. Yuan, W. Ma, C. Chen, J. Zhao, J. Liu, H. Zhu and X. Gao, *Chem. Mater.*, 2007, **19**, 1592–1600.
29 D. Hu, H. Han, R. Zhou, F. Dong, W. Bei, F. Jia and H. Chen, *Analyst*, 2008, **133**, 768–773.
30 H. Zhang, W. Li, Z. Sheng, H. Han and Q. He, *Analyst*, 2010, **135**, 1680–1685.
31 Y. Yang, M. Hori, T. Hayakawa and M. Nogami, *Surf. Sci.*, 2005, **579**, 215–224.
32 J. Xie, Q. Zhang, J. Y. Lee and D. I. C. Wang, *ACS Nano*, 2008, **2**, 2473–2480.
33 E. Hao, R. C. Bailey, G. C. Schatz, J. T. Hupp and S. Li, *Nano Lett.*, 2004, **4**, 327–330.
34 O. M. Bakr, B. H. Wunsch and F. Stellacci, *Chem. Mater.*, 2006, **18**, 3297–3301.
35 V. Giannini, R. Rodríguez-Oliveros and J. A. Sánchez-Gil, *Plasmonics*, 2010, **5**, 99–104.
36 H. Wang and N. Halas, *Adv. Mater.*, 2008, **20**, 820–825.
37 F. Hao, C. L. Nehl, J. H. Hafner and P. Nordlander, *Nano Lett.*, 2007, **7**, 729–732.
38 E. Nalbant Esenturk and A. R. Hight Walker, *J. Raman Spectrosc.*, 2009, **40**, 86–91.

